# Supporting Information

## Amorphous Nickel-Iron Hydroxide Nanosheets for Effective Electroreduction of Nitrate to Ammonia

Xuan Wu[a], Aijing Ma[b], Jun Hu[c], Dan Liu[a,c,d*], Alex T. Kuvarega[d], Bhekie B. Mamba[d], and Jianzhou Gui[a,b,d*]

[a] State Key Laboratory of Separation Membranes and Membrane Processes, Tianjin Key Laboratory of Green Chemical Technology and Process Engineering, School of Material Science and Technology, Tiangong University, Tianjin 300387. China.

[b] State Key Laboratory of Separation Membranes and Membrane Processes, Tianjin Key Laboratory of Green Chemical Technology and Process Engineering, School of Chemical Engineering and Technology, Tiangong University, Tianjin 300387, China.

[c] State Key Laboratory of Separation Membranes and Membrane Processes, Tianjin Key Laboratory of Green Chemical Technology and Process Engineering, School of Chemistry, Tiangong University, Tianjin 300387, China.

[d] Institute for Nanotechnology and Water Sustainability, College of Science, Engineering and Technology, University of South Africa, Florida 1709, Johannesburg, South Africa.

* Corresponding author. E-mail: liudan@tiangong.edu.cn (D. Liu)

* Corresponding author. E-mail: jzgui@hotmail.com (J. Gui)

**Materials and chemicals.** $Fe(NO_3)_3 \cdot 9H_2O$, $Ni(NO_3)_2 \cdot 6H_2O$, $K_2SO_4$, $NaNO_2$, $NH_4Cl$, $KNO_3$, $D_2O$, sulphamic acid, p-aminobenzenesulfonamide, phosphoric acid, N-(1-Naphthyl) ethylenediamine dihydrochloride, Nessler's reagent, and potassium sodium tartrate solution ($NaKC_4H_4O_6$) were purchased from Aladdin (Shanghai, China). Nickle foams were purchased from Taiyuan Yingze District Power source Battery Sales Department. HCl was purchased from Tianjin Fengchuan Chemical Reagent Co, Ltd. $^{15}NH_4Cl$, $K^{15}NO_3$ were purchased from Macklin (Shanghai, China).

**Characterization of Materials.** The morphologies of samples were obtained by scanning electron microscope (SEM, Hitachi S4800) equipped with Energy Dispersive X-Ray Spectroscopy (EDX) and high-resolution transmission electron microscopy (HRTEM, JEOL JEM-2100). The X-ray diffraction (XRD) measurement was characterized through a diffractometer (Bruker D8 Advance A25), using Cu Kα (λ = 0.15468 nm) as the radiation source. The Ultraviolet-visible (UV-Vis) Spectroscopy was measured on Thermo evolution 300 spectrophotometer in quartz cuvettes. The X-ray photoelectron spectroscopy (XPS) data was obtained by a Thermofisher K-alpha spectrometer with monochromatic Al Kα as the radiation source. All the peaks were calibrated using C 1s spectrum at a binding energy of 284.6 eV. The nuclear magnetic resonance (NMR) spectra were recorded on a Bruker AVANCE AV 400MHz spectrometer. The online differential electrochemical mass spectrometry (DEMS) measurements were performed on QAS 100.

**Ion Concentration Detection of Nitrate-N.** 0.2 mL electrolyte was taken from the cathode compartment and was diluted to 1ml with ultrapure water. Then 0.1 mL of the above solution was diluted to 5mL with ultrapure water. Next, 100 μLof 1 M HCl and 10 μL of 0.8 wt% sulphamic acid solution were added to the above 5 mL solution and mixed uniformly. After standing for 20 min, the absorbance of the solution at 220 nm and 275 nm were recorded. The final absorbance is corrected by the following equation: $A = A_{220nm}$ -

$2A_{275nm}$. A series of standard $KNO_3$ solutions with different concentrations were used to obtain the standard concentration-absorbance curve. $KNO_3$ was pre-dried in an oven at 110°C for 2 h.

**Ion Concentration Detection of Nitrite-N.** The color reagent was prepared as follows: First, 4g p-aminobenzenesulfonamide was added to the mixture of 50 mL ultrapure water and 10 mL phosphoric acid ($\rho$=1.70 g $mL^{-1}$) and stirred to dissolve. Next, 0.2g N-(1-Naphthyl) ethylenediamine dihydrochloride was added to the above solution and stirred to dissolve. Finally, the above solution was transferred to a 100mL volumetric flask to make the volume constant. In the detection range, a certain volume of electrolyte was taken out from the cathode compartment and was diluted to 5ml with ultrapure water. Then, the as-prepared color reagent (100 μL) was added to the diluted electrolyte and shaken until the mixture was uniform. The absorbance was recorded at 540 nm after standing for 20 min. A series of standard $NaNO_2$ solutions with different concentrations was used to obtain the standard concentration-absorbance curve.

**Ion Concentration Detection of Ammonia-N.** Nessler's reagent was used as the color reagent to determine the content of ammonia-N. First, within the detection range, a certain volume of electrolyte was taken out from the cathode compartment and diluted to 5ml with ultrapure water. Then, 100 μL potassium sodium tartrate solution ($NaKC_4H_4O_6$, $\rho$=500 g $L^{-1}$) and 100 μL Nessler's reagent were added to the above 5mL diluted electrolyte, and then the solution was shaken until the mixture was uniform. After standing for 20 min, the absorbance was recorded at 420 nm. A series of standard $NH_4Cl$ solutions were used to obtain the concentration-absorbance curve. $NH_4Cl$ was pre-dried in an oven at 110 °C for 2 h.

**Calculation of the Electrochemical Reduction Activity of Nitrate**

The yield of ammonia was acquired by the Eq.1:

$$Yield_{NH_3} = \frac{C_{NH_3} \times V}{M_{NH_3} \times t \times S} \quad (1)$$

The conversion rate of $NO_3^-$ was obtained by Eq. 2:

$$Conversion = \frac{\Delta C_{NO_3^-}}{C_0} \times 100\% \quad (2)$$

The selectivity of $NO_3^-$ and $NO_2$- was acquired by Eq. 3:

$$NH_3\ Selectivity = \frac{C_{NH_3}}{\Delta C_{NO_3^-}} \times 100\% \quad (3)$$

$$NO_2^-\ Selectivity = \frac{C_{NO_2^-}}{\Delta C_{NO_3^-}} \times 100\%$$

The Faradaic efficiency was obtained using Eq. 4:

$$Faradaic\ efficiency = \frac{8F \times V \times C_{NH_3}}{M_{NH_3} \times Q} \times 100\% \quad (4)$$

In the above equations, $C_{NH_3}$ refers to the measured ammonia concentration, V represents the electrolyte volume (50mL) added to the cathode compartment, $M_{NH_3}$ is the $NH_4^+$ molar mass, t refers to the electroreduction time (2 h), S represents the effective geometric area of the working electrode (1 $cm^2$ ), $\Delta c_{NO_3^-}$ represents the concentration difference of $NO_3^-$ before and after electroreduction, $C_0$ is the initial $NO_3^-$ concentration, $C_{NO_2^-}$ refers to the concentrations of nitrite produced, F is the Faradaic constant (96485 C $mol^{-1}$), Q represents the total charge during electrolysis.

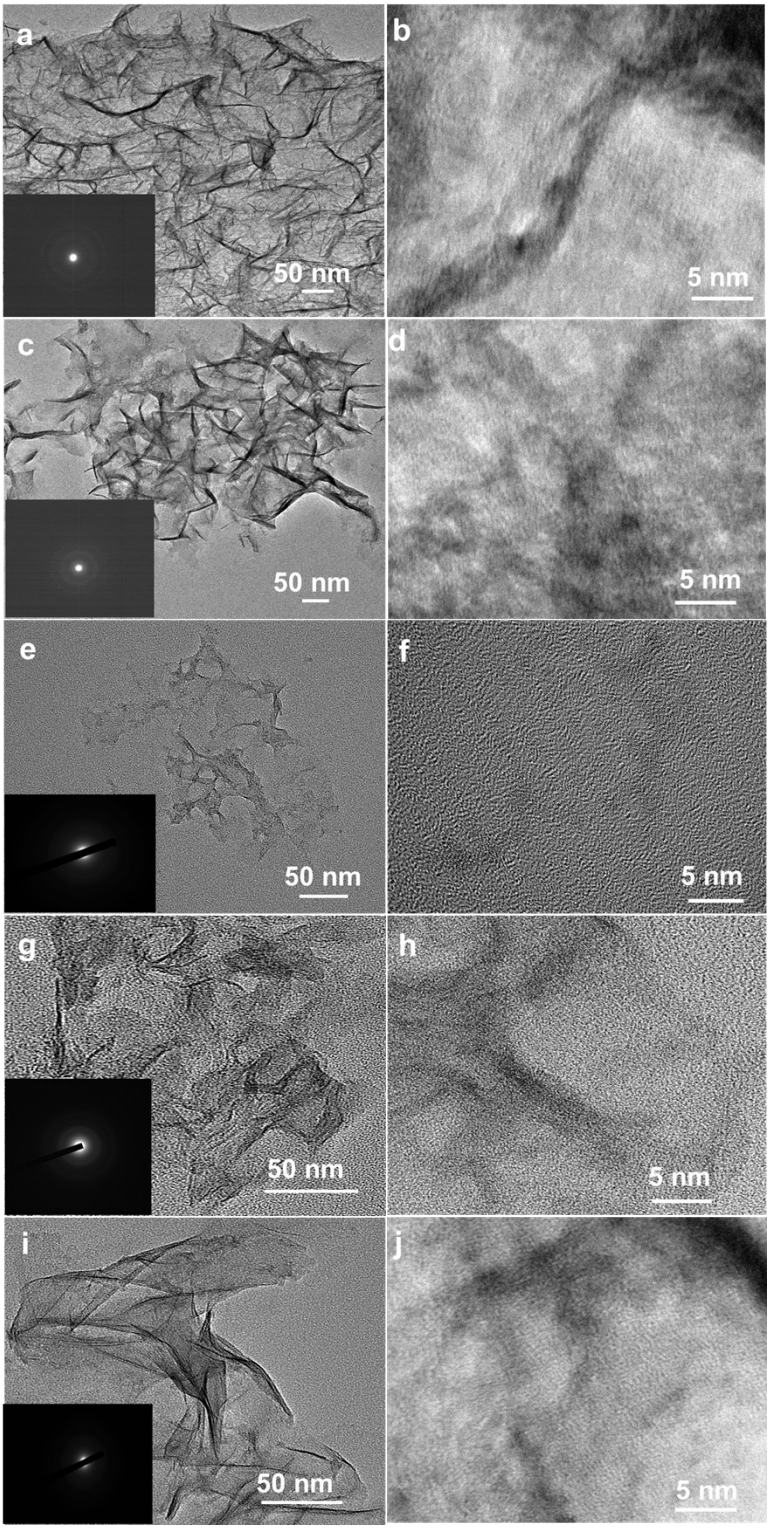


**Figure S1.** TEM and HRTEM images of NiFe hydroxide scraped off from the NiFe / NF (the inset shows the selected area diffraction patterns), (a, b) Ni6Fe0, (c, d) Ni5Fe1, (e, f) Ni1Fe1, (g, h)Ni1Fe5, (i, j) Ni0Fe6.

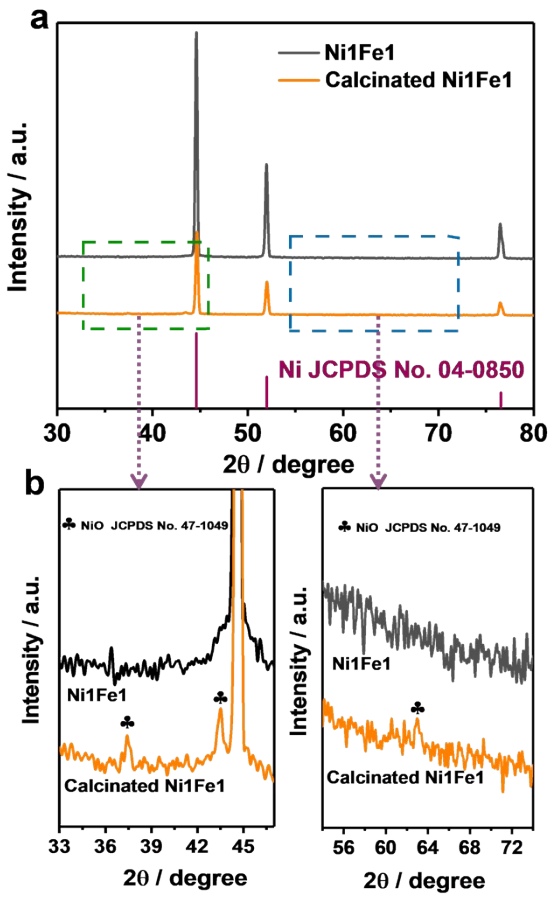


**Figure S2.** (a) XRD patterns of Ni1Fe1 and calcinated Ni1Fe1, (b) The enlarged XRD details patterns of Ni1Fe1 and calcinated Ni1Fe1.

The XRD pattern of Ni1Fe1 only exhibited the diffraction peaks of Ni (JCPDS NO.04-0850) at 2θ of 44.5°, 51.8° and 76.4°. The XRD pattern of calcinated Ni1Fe1 not only exhibited the diffraction peaks of Ni (JCPDS NO.04-0850) at 2θ of 44.5°, 51.8° and 76.4°, but also exhibited the diffraction peaks of NiO (JCPDS NO.47-1049) at 2θ of 37.2°, 43.3°, and 62.9°.

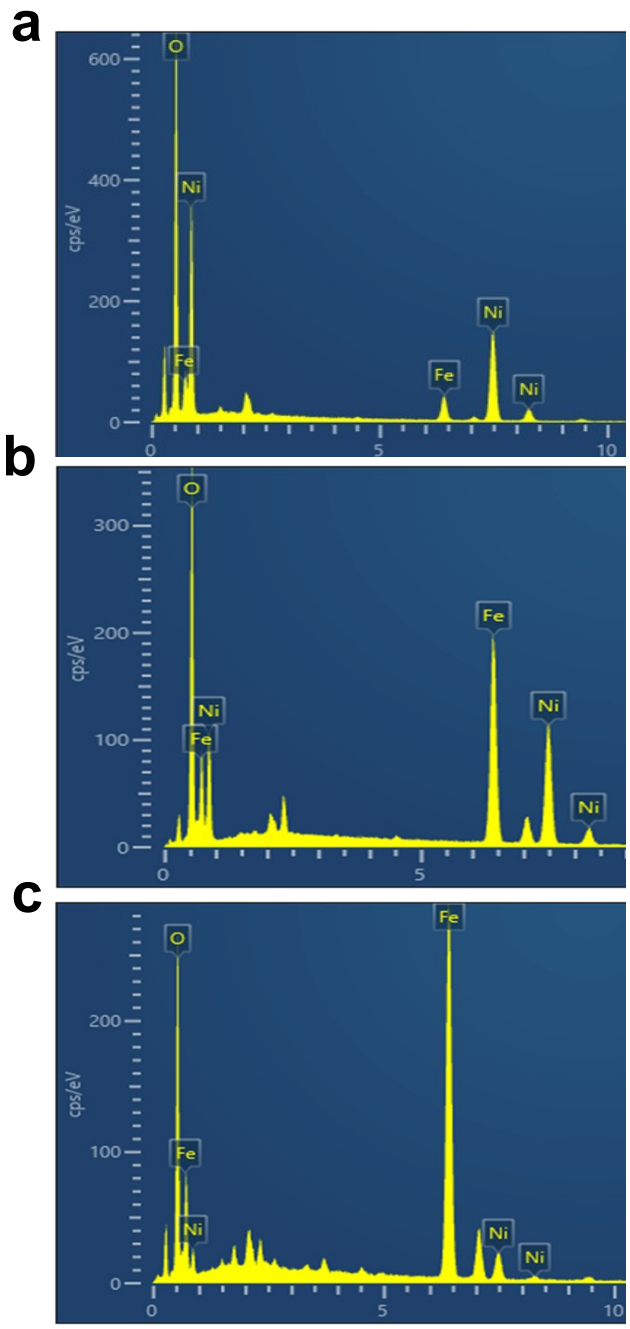


**Figure S3.** EDX of the as-prepared (a) Ni5Fe1, (b) Ni1Fe1, and (c) Ni1Fe5.

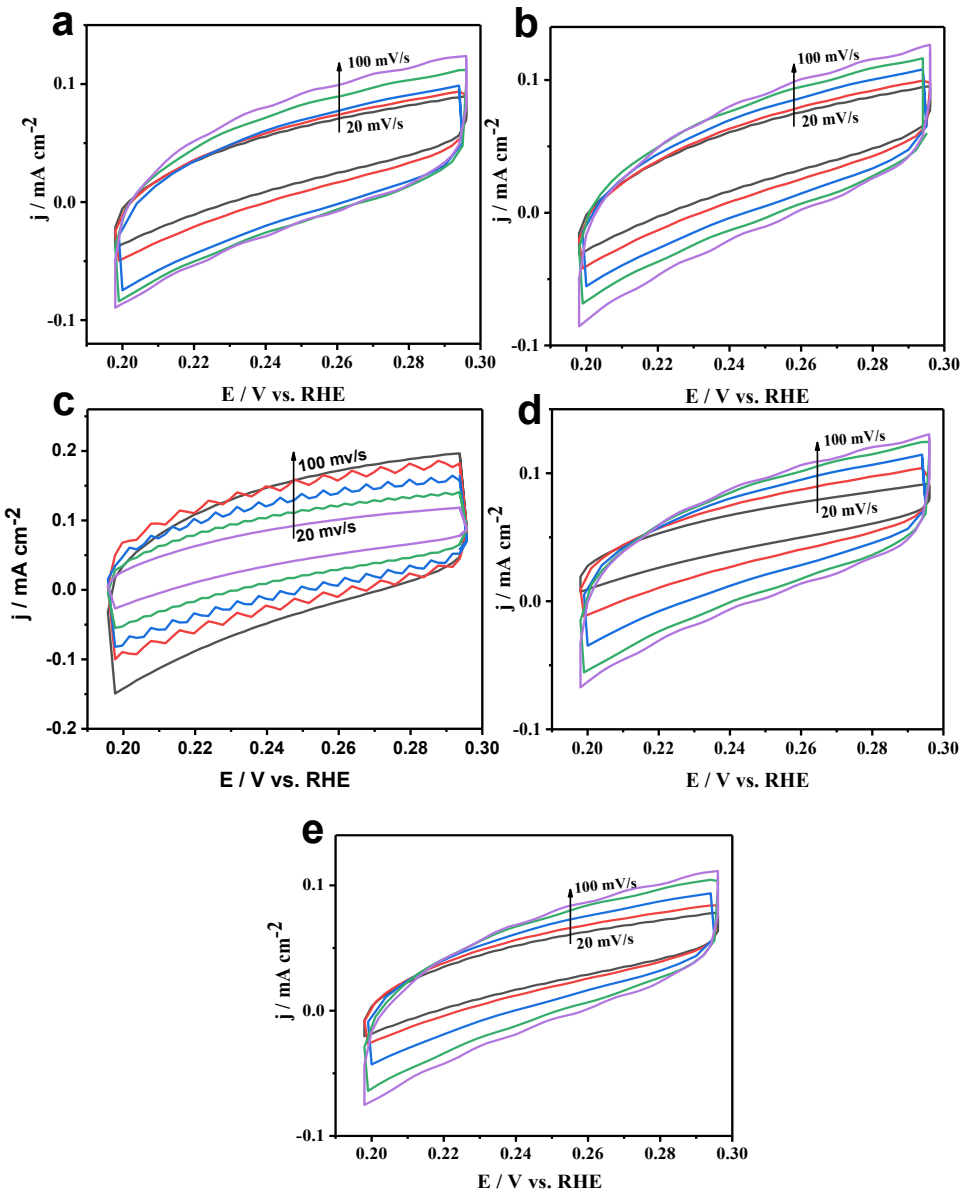


**Figure S4.** CV curves of NiFe hydroxide with various scan rates from 20 to 100 mV $s^{-1}$, (a) Ni6Fe0, (b) Ni5Fe1, (c) Ni1Fe1, (d) Ni1Fe5, (e) Ni0Fe6.

**Table S1.** The Rct values of NiFe hydroxide.

| Sample | Ni6Fe0 | Ni5Fe1 | Ni1Fe1 | Ni1Fe5 | Ni0Fe6 |
|---|---|---|---|---|---|
| Rct (Ω) | 37.3 | 26.3 | 23.7 | 27.4 | 64.5 |

The Rct values of all the electrodes were given in Table S1, which indicated the faster electron transfer process of Ni1Fe1.

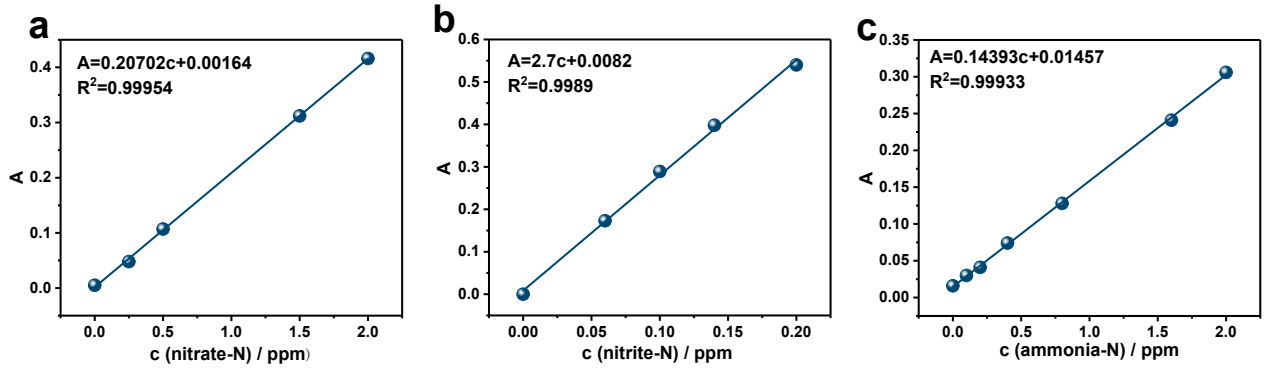


**Figure S5.** The concentration-absorbance calibration curves of (a) nitrate-N, (b) nitrite-N and (c) ammonia-N. The calibration curves all show good linearity.

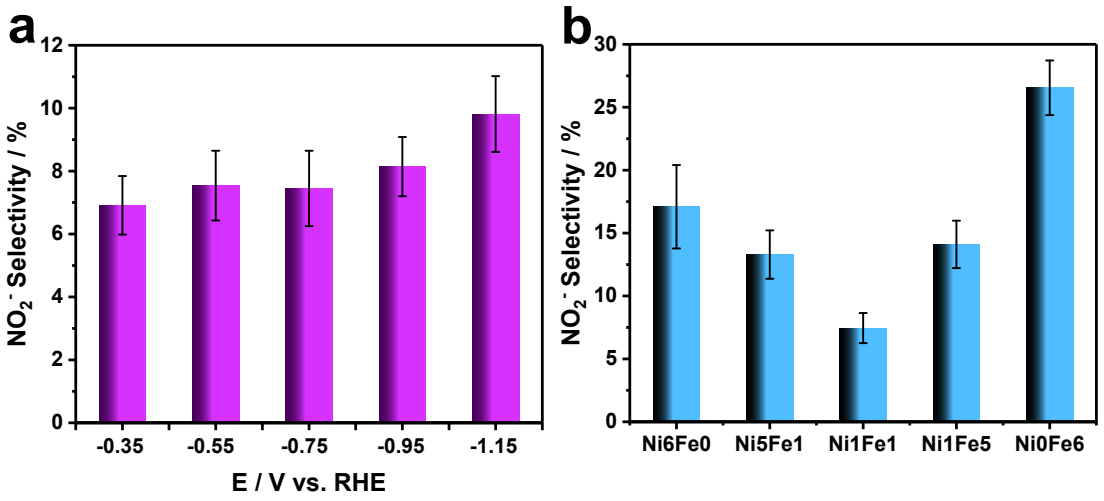


**Figure S6.** (a) Selectivity of $NO_2^-$ over Ni1Fe1 at different potentials. (b) Selectivity of $NO_2^-$ over NiFe hydroxide with different Ni/Fe atomic ratios after potentiostatic test at -0.75V.

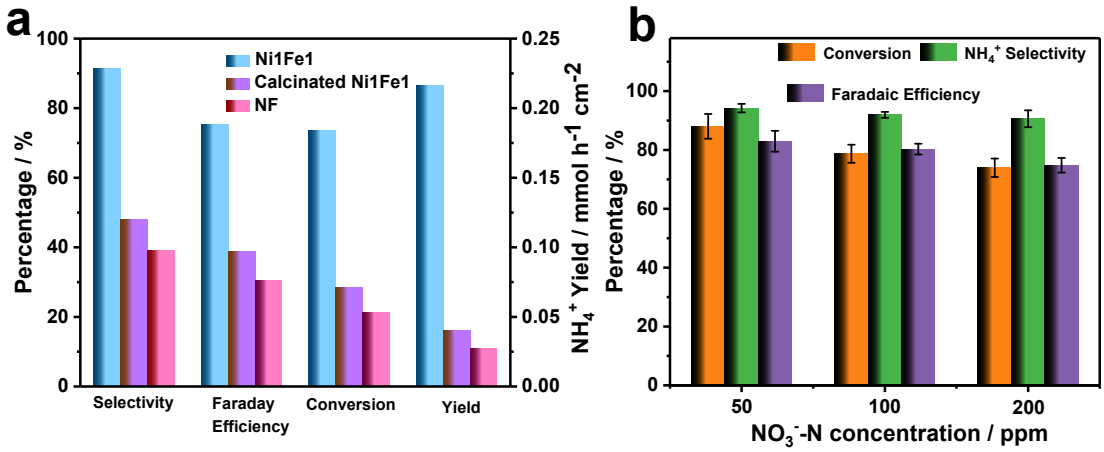

**Figure S7.** (a) The comparisons of Faradaic efficiency, $NO_3^-$ conversion, $NH_4^+$ selectivity, and yield over Ni1Fe1, calcinated Ni1Fe1 and NF at -0.75V vs. RHE, (b) $NO_3^-$ conversion, $NH_4^+$ selectivity and faradaic efficiencies over Ni1Fe1 at different initial $NO_3^-$-N concentrations.

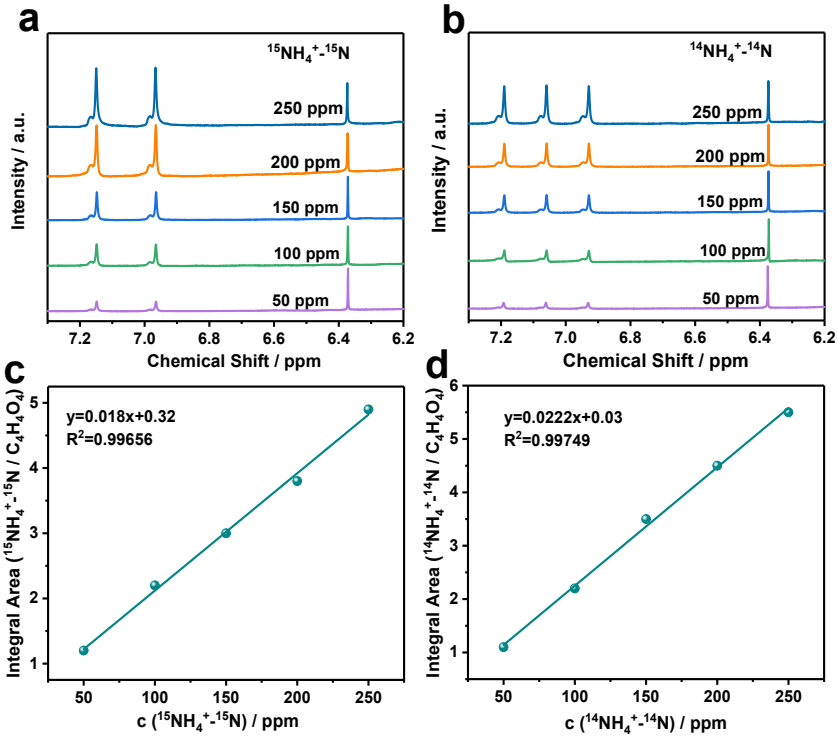


**Figure S8.** (a) $^1H$ NMR spectra of $^{15}NH_4^+$ with different $^{15}NH_4^+$-N concentrations. (b) $^1H$ NMR spectra of $^{14}NH_4^+$ with different $^{14}NH_4^+$-N concentrations. (c) The calibration curve of integral area ( $^{15}NH_4^+$-$^{15}N$ / $C_4H_4O_4$ ) against $^{15}NH_4^+$-$^{15}N$ concentration. (d) The calibration curve of integral area ( $^{14}NH_4^+$-$^{14}N$ / $C_4H_4O_4$ ) against $^{14}NH_4^+$-$^{14}N$ concentration. The peak of maleic acid appears at δ = 6.37 ppm. There were double peaks at δ = 6.97 and 7.15 ppm for $^{15}NH_4^+$, and three peaks at 6.92, 7.06 and 7.19 ppm for $^{14}NH_4^+$.

**Table S2**. Comparison of the quantitative methods between $^1H$ NMR and UV-Vis spectrophotometry for nitrate electroreduction over Ni1Fe1 at -0.75V.

| Quantitative method | Nitrogen sources | Detected ions | Concentration |
|---|---|---|---|
| UV-Vis | $^{14}NO_3^-$ | $^{14}NH_4^+$-$^{14}N$ | 146.88 ppm |
| $^1H$-NMR | $^{14}NO_3^-$ | $^{14}NH_4^+$-$^{14}N$ | 142.79 ppm |
| $^1H$-NMR | $^{15}NO_3^-$ | $^{15}NH_4^+$-$^{15}N$ | 143.33 ppm |

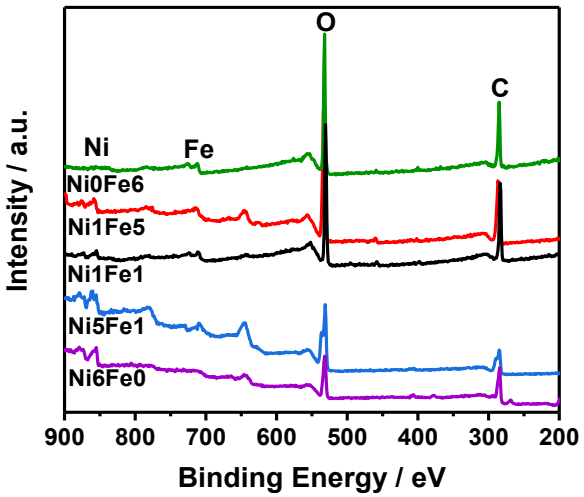


**Figure S9.** Full XPS spectrum of NiFe hydroxide.

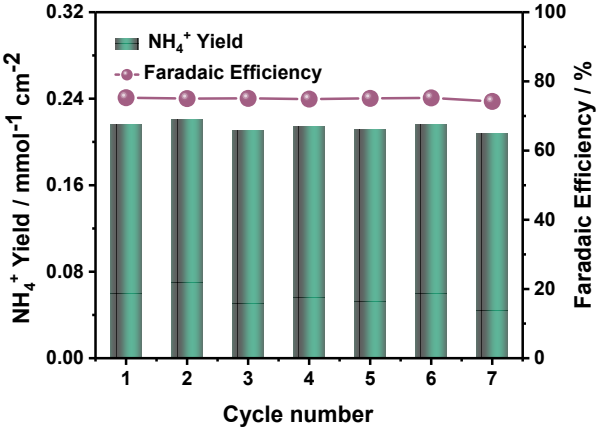


**Figure S10.** $NH_4^+$ yield and Faradaic efficiency over Ni1Fe1 during seven consecutive tests.

**Table S4.** Comparison of ammonia selectivity from nitrate electroreduction.

| catalyst | Electrolyte | Performance | Ref. |
|---|---|---|---|
| Ni1Fe1 hydroxide | 200 ppm $NO_3^-$-N + 0.1 M $K_2SO_4$ t=2h | $S_{NH3}$=91.3% $Y_{NH3}$=0.216 mmol $h^{-1}$ $cm^{-2}$ | This work |
| $TiO_{2-x}$ | 50 ppm $NO_3^-$-N + 0.5 M $Na_2SO_4$ t=2h | $S_{NH3}$=87.1% $Y_{NH3}$= 0.045 mmol $h^{-1}$ $mg^{-1}$ | [1] |
| Amorphous a-$RuO_2$ | 200 ppm $NO_3^-$-N + 0.5 M $Na_2SO_4$ t=2h | $S_{NH3}$=96.42% $Y_{NH3}$= 0.116 mmol $h^{-1}$ $cm^{-2}$ | [2] |

| | | | |
|---|---|---|---|
| Defect-rich Cu nanoplates | 50 ppm $NO_3^-$-N + 0.5 M $K_2SO_4$ t=2h | $S_{NH3}$=85.47% $Y_{NH3}$= 781.25μg $h^{-1}$ $mg^{-1}$ | 3 |
| Amorphous CoBx | 0.1 M KOH +0.05 M $NO_3^-$ t=1h | $S_{NH3}$= / $Y_{NH3}$= 0.787mmol $h^{-1}$ $cm^{-2}$ | 4 |
| Fe SAC | 0.1 M $K_2SO_4$ + 0.5 M $NO_3^-$ t=0.5h | $S_{NH3}$= 75% $Y_{NH3}$= 0.46 mmol $h^{-1}$ $cm^{-2}$ | 5 |
| $Co_3O_4$@NiO | 200 ppm $NO_3^-$-N + 0.5 M $Na_2SO_4$ t=3h | $S_{NH3}$= 62.3% $Y_{NH3}$= 0.00693 mmol $h^{-1}$ $mg^{-1}$ | 6 |
| $Ni_3B$@$NiB_{2.74}$ | 0.1 M KOH +0.1 M $NO_3^-$ t=3h | $S_{NH3}$= / $Y_{NH3}$= 0.198 mmol $h^{-1}$ $cm^{-2}$ | 7 |
| Ni-$Fe^0$@ $Fe_3O_4$ | 50ppm $NO_3^-$ + 10 mM NaCl t=3h | $S_{NH3}$= 10.4% $Y_{NH3}$= / | 8 |
| Cu/$Cu_2O$ NWAs | 200 ppm $NO_3^-$-N + 0.5 M $K_2SO_4$ t=2h | $S_{NH3}$= 95.8% $Y_{NH3}$=0.245 mmol $h^{-1}$ $cm^{-2}$ | 9 |

Note:

$S_{NH3}$ : the selectivity of ammonia;

$Y_{NH3}$: the yield of ammonia.

t: electrolytic time

## REFERENCES


1. R. Jia, Y. Wang, C. Wang, Y. Ling, Y. Yu and B. Zhang, Boosting Selective Nitrate Electroreduction to Ammonium by Constructing Oxygen Vacancies in $TiO_2$, *ACS Catalysis*, 2020, **10**, 3533-3540.
2. Y. Wang, H. Li, W. Zhou, X. Zhang, B. Zhang and Y. J. A. C. Yu, Structurally disordered $RuO_2$ nanosheets with rich oxygen vacancies for enhanced nitrate electroreduction to ammonia, *Angew Chem Int Ed Engl* 2022, **134**, e202202604.
3. Y. Xu, M. Z. Wang, K. L. Ren, T. L. Ren, M. Y. Liu, Z. Q. Wang, X. N. A. Li, L. Wang and H. J. Wang, Atomic defects in pothole-rich two-dimensional copper nanoplates triggering enhanced electrocatalytic selective nitrate-to-ammonia transformation, *Journal of Materials Chemistry A*,

2021, **9**, 16411-16417.

4. Y. B. Shi, S. X. Xu and F. Li, Electrocatalytic nitrate reduction to ammonia via amorphous cobalt boride, *Chem. Commun.*, 2022, **58**, 8714-8717.
5. Z. Y. Wu, M. Karamad, X. Yong, Q. Z. Huang, D. A. Cullen, P. Zhu, C. A. Xia, Q. F. Xiao, M. Shakouri, F. Y. Chen, J. Y. Kim, Y. Xia, K. Heck, Y. F. Hu, M. S. Wong, Q. L. Li, I. Gates, S. Siahrostami and H. T. Wang, Electrochemical ammonia synthesis via nitrate reduction on Fe single atom catalyst, *Nature Communications*, 2021, **12**, 10.
6. Y. T. Wang, C. B. Liu, B. Zhang and Y. F. Yu, Self-template synthesis of hierarchically structured Co3O4@NiO bifunctional electrodes for selective nitrate reduction and tetrahydroisoquinolines semi-dehydrogenation, *Sci. China-Mater.*, 2020, **63**, 2530-2538.
7. L. Li, C. Tang, X. Cui, Y. Zheng, X. Wang, H. Xu, S. Zhang, T. Shao, K. Davey and S. Z. J. A. C. Qiao, Efficient nitrogen fixation to ammonia through integration of plasma oxidation with electrocatalytic reduction, 2021, **133**, 14250-14256.
8. D. Yin, Y. Y. Liu, P. F. Song, P. Chen, X. Liu, L. K. Cai and L. H. Zhang, In situ growth of copper/reduced graphene oxide on graphite surfaces for the electrocatalytic reduction of nitrate, *Electrochimica Acta*, 2019, **324**, 9.
9. Y. T. Wang, W. Zhou, R. R. Jia, Y. F. Yu and B. Zhang, Unveiling the Activity Origin of a Copper-based Electrocatalyst for Selective Nitrate Reduction to Ammonia, *Angew. Chem.-Int. Edit.*, 2020, **59**, 5350-5354.